Exosomal Mir-21 Derived from Umbilical Cord Mesenchymal Stem Cells Promotes Angiogenesis by Activating SPRY1/PI3K/AKT Pathway and Contributes New Bone Formation in a Rat Model.

Yuntong Zhang
Changhai Hospital
Xiaoqun Li
Changhai Hospital
Yang Xie
Changhai Hospital
Yan Xia
Changhai Hospital
Panfeng Wang
Changhai Hospital
Zichen Hao
Changhai Hospital
Shuo Fang
Changhai Hospital
Shuogui Xu (mone1030@163.com)
Changhai Hospital https://orcid.org/0000-0002-0329-9330

Research

Keywords: uMSC-Exos, miR-21, SPRY1, PI3K-AKT, bone healing

Posted Date: August 2nd, 2021

DOI: https://doi.org/10.21203/rs.3.rs-730503/v1

Abstract

Background: Delayed atrophic healing and non-union remain the most difficult types of complications to treat and can lead to numerous re-operations and high socioeconomic cost. Exosome derived from MSCs is a promising strategy in the treatment of fracture. However, it's still not fully clear in the underlying mechanisms.

Methods: In this study, we first elucidated the underlying mechanism of umbilical cord MSC (uMSC)-Exo-induced angiogenesis in bone regeneration and fracture repair. RT-PCR, luciferase reporter, western blot and immunofluorescence in situ hybridization assay were performed to identify the expression of related genes and pathways in uMSC-Exo. Proliferation, tube formation and transwell migration assay were used to evaluated the effects of uMSC-Exo in vitro. A rat calvarial defect model was used to evaluated the effects of uMSC-Exo in vivo.

Results: We found that, miR-21 was the most abundant miRNA in the uMSC-Exos. In vivo and in vitro experiments demonstrated that, the uMSC-Exo could promote the migration, angiogenic and capacity of HUVECs via miR-21, inhibition of miR-21 could attenuate the effects of uMSC-Exos. For mechanical study, we found that, exosomal miR-21 derived from uMSCs activates PI3K/AKT signalling by targeting SPRY1 in HUVECs, SPRY1 knockdown could promote the PI3K/AKT activation and HUVEC proliferation, migration and angiogenesis. In addition, exosomal miR-21 derived from uMSCs enhanced local microvascular network formation and bone regeneration in vivo.

ConclusionIn: In conclusion, we firstly reported that uMSC-derived exosomes as a ready-made regenerative medicine therapy to bone healing.

Introduction

Effective treatment for fracture remains challenging, and poor or impaired recovery from fracture is an increasingly severe problem in an ageing society[1, 2]. In approximately 5–10% of cases, fracture union is delayed or compromised and can lead to numerous re-operations and high socioeconomic costs [3, 4]. Throughout the processes of bone regeneration and fracture healing, angiogenesis is indispensable[5]. The effects of drug intervention on the regeneration of intractable sequestrum or atrophic callus are not adequate by reason of poorly vascularized tissue surrounding the haematoma at the fracture site[5, 6]. Thus, factors of angiogenesis, which is the growth of new vasculature, may be promising therapeutic targets for fracture healing and crucial to the development of more-efficacious biological strategies.

Evidence has shown that, application of mesenchymal stem cells (MSCs) could be a potential therapeutic strategy to induce bone regeneration[7, 8]. Nevertheless, it remains limitary for the clinical use of stem cells due to many risk factors, including undesirable immune reaction, thrombosis, and even tumour formation [9, 10]. Various studies have shown that exosomes derived from MSCs plays an important role in clinical therapy, which are emerging as components of a cell-free regenerative medicinal approach to tissue repair because of their stem cell-like pro-regenerative properties and the prospect of circumventing

some of the drawbacks of MSCs use[11, 12]. The results from our previous study demonstrated that umbilical cord mesenchymal stem cells-derived exosomes (uMSC-Exos) promoted angiogenesis in a rat femur fracture model[13]. The pro-angiogenic function of endothelial cells has been induced, and several pro-angiogenic factors, such as HIF-1α, have been upregulated. These results are consistent with those of several recent studies[14–16]. But the underlying mechanisms of uMSC-Exo-promoted angiogenesis in bone healing are not fully understood.

Exosomes are reported as nano-carriers ranging from 40–100 nm in diameter, which contains a various of genetic information, such as mRNA and miRNA. Among all the molecules possibly contained within exosomes. A growing body of evidence indicates that miRNAs in exosomes regulate the cell activity[17]. For instance, uMSC-derived exosomes promoted wound healing while preventing scar formation via the intercellular transfer of specific miRNAs, such as, miR-21, miR-23a, miR-125b, and miR-145[18]. To further investigate the exosome-related cell-cell communication between endothelial cells and uMSCs, we analyzed the critical miRNAs of uMSC-Exos and evaluated their roles in endothelial cell biological function. In addition, the target genes and molecular signalling pathways in recipient cells were revealed. Ultimately, we verified the hypothesized molecular mechanisms and demonstrated the possible optimal therapeutic effects of uMSC-Exos application in a cranial defect model.

Materials And Methods

uMSC and HUVEC cultures

uMSCs were cultured in α-MEM culture medium added by 15% FBS and 4% penicillin and streptomycin (Gibco, Grand Island, USA). The human umbilical cord vein endothelial cells (HUVECs) were separated and harvested as previously described[1]. The cell culture protocols were authorized through Ethical Committee of the Navy Medical University. Briefly, uMSC were obtained from 3 healthy donors respectively and were collected to get uMSC-Exos.

Quantitative real-time PCR

Total RNA of HUVECs transfected with uMSC-Exo-anti-miR-NC, uMSC-Exo-anti-miR-21 and uMSC-Exo was isolated by TRIzol solution followed by the informations of manufacturer. The concentration of the total RNA solution were measured by a commercial kit (Thermo Fisher Scientific). Then, we reversed the first-strand cDNA via 2 μg RNA with a cDNA commercial kit (Thermo). Quantitative real-time PCR (qRT-PCR) was conducted with a 25-μL reaction volume (Detailed steps are visible in the supplementary material).

Purification and identification of exosomes derived from uMSCs

Firstly, the uMSCs were seeded at 1.5×10^5 cells in a T25 polystyrene culture flasks (Corning) with 5 mL of α-MEM culture medium for 24 hours adherence. After that, the flasks were washed for 3 times by PBS and the culture medium with exo-free-FBS [3] was added in them. After 48 h, the freshly collected supernatant

was centrifuged at 1500×*g* for 5 min at room temperature and then 10000×*g* for half an hour at 4 ℃ to remove the impurities. Exosomes were precipitated by an ExoQuick-TC kit (ExoQuick-TC) followed by the manufacturer's instructions. The identity of the exosomes was determined or confirmed by their binding affinity for CD63, CD81, and CD9 antibodies (Abcam, USA), which were reported to be specific exosome biomarkers[4, 5].

RNA interference

The miR-21 mimic sequences Forward (5'-tacctcgagtgtctgcttgttttgcct-3') and Reverse (5'-tacgaattctgtttaaatgagaacatt-3'), miR-21 inhibitor sequence (5'-ucaacaucagucugauaagcua-3'). The sequence of the negative control oligonucleotide (5'-caguacuuuuguguaguacaa-3') were provided by RiboBio (Shanghai, China). Cell transfection process was performed following the manufacturer's instructions (Detailed steps are visible in the supplementary material).

Immunofluorescence in situ hybridization assay of miR-21

To perform immunofluorescence in situ hybridization assays, HUVECs were treated with UEFS and uMSC-Exo-miR-21, seeded on coverslips and fixed by 4% PFA at room temperature for 5 min. After that, the coverslips were treated with blocking reagents (Sigma-Aldrich, USA) for 15 min. Next, a fluorescent probe for miR-21 and the scramble control was hybridized with the HUVEC slides according to well-established consecutive procedures. After two hours of incubation, the hybridization was stopped via stopping buffer (Sigma-Aldrich, USA) and the nuclei were counterstained with DAPI. After washing three times, the slides were dehydrated and photographed under an immunofluorescence microscope at 200× magnification.

Luciferase reporter assay

We predicted the potential binding sites of miR-21 to get the fragments sequences on the biological prediction website (http://www.microrna.org), and the SPRY1 was proved as a target gene to miR-21. The chemical synthesis was performed, after that, luciferase reporter plasmid were cotransfected into HEK293 cells. Cells were incubated for 36 hours in a 12-well plate. After transfection, the cells were examined by a commercial dual-luciferase reporter assay kit (Nanjing, Jiangsu, China), and the luciferase activity was detected.

Western blotting

HUVECs treated with uMSC-Exo-anti-miR-NC, uMSC-Exo-anti-miR-21 or uMSC-Exo were washed with ice-cold PBS three times after the culture medium was removed. The total protein content was extracted from the HUVECs by highly concentrated RIPA lysis buffer and detected by the BCA protein assay kit. 10 μg of total protein was added to SDS-PAGE and transferred into a PVDF membrane. A 5% non-fat milk solution prepared with 1×TBST was utilized to block the PVDF membrane for one hour at 4 ℃. Then, the PVDF membrane was incubated with the following specific primary antibodies for 1 h at room temperature: anti-PI3K (1:1000, CST, USA), anti-SPRY1 (1:1000, CST, USA), anti-VEGFA (1:1000, CST, USA), anti-HIF-1α (1:1000, CST, USA), anti-p-AKT (1:1000, CST, USA), anti-AKT (1:1000, CST, USA), anti-β-actin (1:5000, CST, USA), anti-CD9 (1:1000, CST, USA), anti-CD81 (1:1000, CST, USA) and anti-CD63 (1:1000, CST, USA). The

reaction was captured on BioMax film (Kodak, Rochester, NY, USA). β-Actin or CD9 was the internal control.

Proliferation assay:

To put it simply, 1×10^5 HUVEC cells/well were incubated in a 24-well plates and treated with uMSC-Exos (10 μg/well), uMSC-Exo-anti-miR-NC and uMSC-Exo-anti-miR-21. A group of HUVECs with the same volume of PBS served as the control group. At different points in time, 15 μL of CCK-8 solution (Kyushu Island, Japan) was put into the well. Cells were incubated at room temperature for 2 hours. The absorbance of cells was detected at 450 nm by a microplate reader.

Tube formation assay (in vitro angiogenesis)

Cryopreserved HUVECs were seeded in a tissue culture flask. A commercial tube formation assay kit (Cell Biolabs, USA) was used to assess in vitro angiogenesis within 18 h of cell seeding. Thawed ECM gel was added to a plate and cultured for 1 hour. After that, HUVECs in suspension were added to the solidified ECM gel and cultured for 12 h at room temperature. We added uMSC-Exo-anti-miR-NC, uMSC-Exo-anti-miR-21, uMSC-Exo (100 μg/mL; 200 μg/well) to the HUVEC tube formation system. We examined and imaged the tube formation at 12 h and 24 h using a light microscope in a high magnification field.

Scratch test

A total of 2×10^5 HUVECs were put into a 12-well plate and incubated until confluent. Using pipette tip, we made a straight scratch in the monolayer to simulate a wound. The HUVECs were transfected with PBS, uMSC-Exo-anti-miR-NC, uMSC-Exo-anti-miR-21, and uMSC-Exo (100 μg/mL; 200 μg/well). After 0 h, 6 h, 12 h and 24 h of incubation, the width of the wound was photographed and cell migration was evaluated using an optical microscope (Leica, Germany). The width of the wound at 0 h was set as a negative control. Moreover, the wound width at each time point was normalized to that at 0 h and compared to the width measured at other time points. The assay was repeated at least three times.

Transwell migration assay

For the Transwell assay, 1×10^4 cells/well (three replicates per group) were suspended in low serum medium (5% FBS) and seeded into the upper chamber of Transwell 24-well plates (Corning, Corning, NY, USA) with 8 μm pore filters. Then, complete medium (containing 10% FBS) supplemented with PBS, uMSC-Exo-anti-miR-NC, uMSC-Exo-anti-miR-21 and uMSC-Exo (100 μg/mL; 200 μg/well) was added to the lower chamber. 12 hours later, the extent of cell migration was calculated by using an optical microscope.

Rat calvarial defect model

All surgical procedures were performed under general anaesthesia using intraperitoneal injection of chloral hydrate (4%, 9 mL/kg body weight), and post-operative analgesic care was ensured with the administration of tramadol. All operations were performed under sterile conditions. Classical porous β-TCP scaffolds (5-mm diameter and 2-mm depth) with an average pore size of 500 μm and 75% porosity

and a HyStem-HP hydrogel (catalogue: GS315, Glycosan BioSystems, Salt Lake City, UT, USA) were used as the exosome carriers. Aliquots of 200 μg of MSC-Exos with or without overexpressed miR-21 (uMSC-Exo group and uMSC-Exo-miR-21 + group, respectively) were dropped onto each scaffold under sterile conditions and lyophilized for at least 4 h, and the scaffold generated with phosphate-buffered saline was used as a negative control group (blank group). The scaffolds were implanted into calvarial defects in adult male Wistar rats (weighing 400-450 g) as previously described[15]. All surgeries were performed according to a protocol approved by the Institutional Animal Care Committee at the Navy Medical University.

Micro-CT analysis

The rats were sacrificed successively at predetermined time points over 6 weeks. The cranium of each rat was obtained and fixed in a 4% paraformaldehyde solution before further analysis. The vascularity was detected using a micro-CT-based method as described previously[13] (Detailed steps are visible in the supplementary material). The defect area was analysed to calculate the percentage of new bone volume (BV), tissue volume (TV), BV/TV, vessel volume (VV), and bone mineral density (BMD) (n = 3).

Histological analysis.

Specimens and intact surrounding tissues were further processed to obtain 6 μm paraffin-embedded sections. Haematoxylin/eosin (HE) staining was conducted for histological assessments. SPRY1, VEGFA and CD31 expression was analyzed by immunohistochemistry with the appropriate antibodies (Abcam, USA). Ultimately, all the sections were observed with a light microscope (Leica, Germany), and then the levels of VEGFA, CD31 and SPRY1 expression were analyzed in each sample via Image J software.

Statistical analysis

Each assay in this study was performed in triplicate. All experimental data were statistically analysed by SPSS software and presented as the mean ± SD. A two-sided Student's *t*-test was performed to compare the differences between two groups. The difference was considered as significant when the *p* value was less than 0.05 or 0.01.

Results

1. miR-21 was the most abundant miRNA in the uMSC-Exos and was shuttled directly from uMSCs to HUVECs via exosomes.

Accumulating evidence demonstrates that exosomes can fuse with the target cell membrane to deliver various messengers, such as miRNA, proteins or lipids, thereby facilitating signal cross talk between different kinds of cell types to control multiple target genes[19]. Although the miRNA profiles of some

typical cancer-derived exosomes have been thoroughly illustrated[20], the exosome miRNA signatures in uMSCs and other cells have not been fully elucidated and need to be investigated further. To characterize the uMSC-derived exosomal miRNAs, we analysed the expression levels of microRNAs in uMSC-Exos via high-throughput sequencing patterns with a HEK293-Exos as controls. The microRNA expression patterns in uMSCs were then analysed using a GEO data set (GSE46989, http://www.ncbi.nih.gov/geo/). We demonstrated that the specific miRNA signature in uMSC-Exos that was completely different from that of HEK293-Exos and uMSCs. The miR-21 was expressed at the highest level among the total miRNAs in the uMSC-Exos (Figure 1A, B). Based on the top 10 expression of miRNAs in the uMSCs and uMSC-Exos, we found that miR-21-5p, miR-100-5p, miR-125b-5p, and let-7f-5p were also highly expressed in the uMSCs, with miR-21 accounting for the highest proportion in both the maternal cells and the exosomes (Figure 1C, D).

To verify our conjecture, qRT-PCR was used to evaluate the 10 most abundant miRNAs in uMSC-Exos and their pre-miRNAs expression levels in the HUVECs treated with uMSC-Exos or HEK293-Exos for 48 h. Only the expression of miR-21-5p in the uMSC-Exo group was significantly increased compared with that of the other miRNAs, while the pre-miRNAs were not affected (Figure 1E, F). This result confirmed that an amount of mature miR-21 sufficient to perform biological functions was transported into the HUVECs by the uMSC-Exos. Exosomes have been shown to perform biological roles similar to that of their maternal cells. Moreover, the paracrine function of uMSCs is the most critical in the field of tissue regeneration[11]. Therefore, we hypothesized that the role of uMSCs may be associated with the secretion of exosomes that deliver miR-21 to target cells.

To investigate whether exosomes mediate miR transfer, the expression of miR-21 was measured after MSCs were treated with 10 μM GW4869 (an exosome release inhibitor) for 48 h in conditioned medium (CM). GW4869 is a cell-permeable symmetrical dihydroimidazole-amide compound that acts as a potent, specific, non-competitive inhibitor of membrane neutral sphingomyelinase (nSMase) which has been reported to markedly reduce exosome release[21, 22]. As shown in Figure 1G, the levels of miR-21 in the CM collected from MSCs treated with GW4869 were significantly decreased compared with those in the CM obtained from control uMSCs. In addition, the expression of miR-21 in HUVECs treated with GW4869-CM for 48 h was also significantly decreased compared to that of HUVECs treated with uMSC-CM (Figure 1H), indicating that exosomes mediated the miRNA transport between the uMSCs and HUVECs. To improve the visibility of the results, uMSC-Exos fluorescently stained with PKH67 were cultured with HUVECs for 48 h. In addition, FAM was conjugated to miR-21 (miR-21-FAM) in the uMSC-Exos to trace miR-21 by in situ hybridization. The immunofluorescence showed that the green exosomes were concentrated mainly near the nuclei of the HUVECs and the location of the ectogenic miR-21 (red spots) was consistent with that of the exosomes. However, exosome and miRNA components were not detected in the uMSC-Exo-free supernatant (UEFS) (Figure 1I).

All these results indicated that miR-21 might be contained in the exosomes excreted by the uMSCs, a finding that supports our hypothesis that uMSCs deliver miR-21 directly to the target cell for biological function.

2. Preparation and identification of uMSC-Exos with inhibited miR-21

To validate the critical roles of miRNAs, inhibition experiments are more illustrative than overexpression experiments. We developed a strategy to stably inhibit miRNAs inside the uMSC-Exos. The uMSCs were transfected with antagomir RNA-21 to block miR-21 (uMSC-Exo-anti-miR-21) or a scrambled antagomir as a negative control (uMSC-Exo-anti-miR-NC). The exosomes were then extracted using a kit, and the qRT-PCR results demonstrated that the uMSC-Exo-anti-miR-21 group had a significantly downregulated level of miR-21 and the level was not changed in the control groups (Figure 2A).

The exosomes in the three groups were successfully precipitated by an ExoQuick-TC kit (ExoQuick-TC, System Biosciences) according to the manufacturer's instructions. The morphology of the purified exosomes was observed by using transmission electron microscopy (TEM). Whether exposed to the inhibitor or not, all exosomes had a saucer-like shape with a diameter ranging from 40 to 100 nm (Figure 2B). The diameter of the exosomes was determined with a NanoSight LM10 instrument (NanoSight, Amesbury, U.K., http://www.nanosight.com) (Figure 2C). The markers of the exosomes, namely, CD9, CD63 and CD81, were also detected by Western blotting, and the results showed that compared with the amounts in the UEFS, the CD9, CD63 and CD81 levels were enriched in the exosome samples (Figure 2D). This finding indicates that the remodelling and extraction of the uMSC-Exos were effective and reliable.

3. Effects of exosomal miR-21 on the cellular functions of HUVECs

We evaluated the role of miR-21 in uMSC-Exo by in vitro and in vivo experiments. All phenotypic experiments were conducted with four groups: The uMSC-Exo-anti-miR-NC, uMSC-Exo-anti-miR-21, uMSC-Exo groups and a blank group (HUVECs with PBS). Previous reports demonstrated that miR-21 has an effect on cancer cell proliferation[6]. However, the mechanism of uMSC exosomal miR-21 in HUVEC proliferation remains unknown. The CCK-8 analysis showed that exosome stimulation resulted in a significant increase in HUVEC proliferation, although the effect was reduced by the miR-21 inhibitor (Figure 3A).

To determine whether exosomal miR-21 modulates cell migration, HUVECs were incubated with PBS, uMSC-Exo-anti-miR-NC, uMSC-Exo-anti-miR-21 or uMSC-Exo and the monolayer was disrupted with a straight scratch. After 12 h and 24 h, the wound width in the culture of each group was photographed (Figure 3B). We observed that at the same time point (12 h or 24 h), the migration rate of HUVECs in the uMSC-Exo-anti-miR-21 group was significantly lower than that of the other two groups (uMSC-Exo and uMSC-Exo-anti-miR-NC) and similar to that of the blank control group. Furthermore, we conducted a Transwell assay, and the results showed that the number of migrating HUVECs was reduced by approximately one-half after the treatment with exosomal miR-21 inhibitor (Figure 3C). These results indicated that the loss of miR21 uMSC-Exo no longer enhanced the migration capacity of HUVECs.

The tube formation assay was performed to obtain direct evidence of the angiogenic function of miR-21 in HUVECs. The results showed that there were newly growing branch points and tube lengths in the uMSC-Exo group and uMSC-Exo-anti-miR-NC group that formed in a time-dependent manner while the tube formation in the group with inhibited miR-21 was weak (Figure 4A). Thus, these results directly demonstrated the angiogenic role of uMSC-Exos in HUVECs, which could be suppressed by the miR-21 inhibitor.

The role of miR-21 derived from uMSC-Exos in promoting angiogenesis was verified by an in ovo angiogenesis assay. Eight-day-old embryonated chicken eggs were used for different treatments once a day. Two days after treatment, the CAM was assessed for changes in the number and length of blood vessels. The data showed that uMSC-Exo-anti-miR-21 was able to impair in ovo neovascularization, and the value was two-fold less than that of the other two control groups as assessed on the tenth day. In addition, on the 12th day, the density of the vessels increased compared to that observed in previous days, although the inhibition effect was most obvious in the experimental group (Figure 4B). This finding is consistent with our in vitro test results showing that exosomes with inhibited miR-21 have a significantly reduced effect on angiogenesis.

4. Exosomal miR-21 derived from uMSCs activates PI3K/AKT signalling by targeting SPRY1 in HUVECs

VEGFA has been reported to have an essential role in HUVEC-mediated angiogenesis[7]. Various types of evidence verified that VEGF increases the vascular density through SPRY1 and that SPRY1 negatively regulates angiogenesis. SPRY1 was predicted to be a potential target gene of miR-21 by the microRNA (http://www.microrna.org/) and TargetScan (http://www.targetscan.org/) databases. However, whether uMSC-Exo-miR-21 plays a critical role through SPRY1 in HUVEC-mediated angiogenesis has not been reported, and the signalling pathways are also unknown. In this study, the luciferase reporter assay results showed that miR-21-5p can bind to the 3’-UTR of SPRY1 and suppress the transcription of SPRY1 when the miR-21 overexpression vector was transfected into HEK293 cells (Figure 5A, B).

An inhibitory effect of SPRY1 on angiogenesis, which is induced by PI3K/AKT activation in cancer cells, has been demonstrated[23]. Thus, we used the method of SPRY1 knockdown to identify the downstream pathway in HUVECs. The qRT-PCR results indicated that the mRNA level of SPRY1 increased dramatically by approximately two-fold when uMSC-Exo-anti-miR-21 was used to interfere with HUVECs, and no difference was observed between the other two groups (Figure 5C). The mRNA level of the downstream gene P13K showed the opposite trend under the same conditions, although the changes in the total AKT levels were not apparent. The miR-21 inhibitor markedly decreased the upregulated mRNA levels of HIF-1α and VEGFA (genes related to vascularization) induced by exosomes T (Figure 5D). These results were consistent with those of the Western blot assay (Figure 5E). Notably, uMSC-Exo and uMSC-Exo-anti-miR21 induced significant increases in the phosphorylation of Akt while the total AKT remained unchanged.. Hence, we suggested that uMSC-Exo-miR-21 suppressed the expression of SPRY1 and

promoted the hyperactivation of AKT (p-AKT), leading to increased angiogenesis by regulating the SPRY1/PI3K/AKT signalling axis in the HUVECs. Thus, the activation of SPRY1/PI3K/AKT pathways may be the underlying mechanism by which miR-21 containing uMSC-Exos enhance angiogenesis.

5. SPRY1 knockdown increases PI3K/AKT activation and HUVEC proliferation, migration and angiogenesis.

To confirm the key role of SPRY1 in angiogenesis and assess whether knocking down the expression of SPRY1 can achieve similar effects as uMSCs-Exo on angiogenesis, we used siRNA to inhibit the expression of SPRY1 in HUVECs. First, we examined the inhibitory efficiency of these siRNAs by qRT-PCR and Western blot (Figure 6A, B), and the most effective siRNA (siSPRY1 #1) was used for the following functional assays. Next, HUVECs were transfected with SPRY1 siRNAs#1 in culture for 24 h. PI3K/AKT activation and the target genes (VEGFA and HIF-α) were determined by qRT-PCR and Western blot. As expected, we observed an increased level of PI3k, AKT, VEGFA and HIF-1α in the uMSC-Exo+siRNA-SPRY1$^{\#1}$ group. (Figure 6C, D)

Because SPRY1 was found to decrease PI3K/AKT activation, we then tested whether SPRY1 knockdown truly stimulates HUVEC-induced angiogenesis. To determine the extent of HUVEC migration, the scratch experiment showed that at 12 h and 24 h, the HUVECs in the uMSC-Exo+siRNA-SPRY1$^{\#1}$ group migrated at a faster rate, although the number of cells that migrated increased in both groups (Figure 6E). Similarly, the tube formation data showed that after SPRY1 was silenced, the number of branches and blood vessels more than doubled (Figure 6F).

Taken together, the data from our in vitro functional assays on HUVECs suggested that SPRY1 knockdown increased PI3K/AKT activation and HUVEC proliferation, migration and angiogenesis.

6. Exosomal miR-21 derived from uMSCs enhanced local microvascular network formation and bone regeneration in vivo

To study the influence of exosomal miR-21 on bone formation in vivo, the rat cranial bone defect model was carried out for a duration of 6 weeks. In particular, to evaluate the potential therapeutic role of regulated exosomes in bone healing, we developed an experimental group with exosomes that overexpressed miR-21 (uMSC-Exo-miR-21+) and compared the findings with those of the uMSC-Exo group and the negative control (NC) group.

Then, micro-CT and histological analyses were used to evaluate the extent of calvarial defect repair in the three groups (Figure 7A). Similar to our previous study results in a femur fracture model, the administration of uMSC-Exos led to an obvious increase in the amount of new bone formation compared

with that in the NC group. Moreover, compared to both the uMSC-Exo and the control groups, treatment with uMSC-Exos with overexpressed miR-21 led to a significant increase in the bone volume (BV), BV/TV and bone mineral density (BMD). Vascular growth within the bone callus was evaluated by imaging of contrast-perfused, decalcified specimens. The vessel volume was remarkably increased in the uMSC-Exo-miR-21+ group.

H&E staining was used to observe the microscopic bone and soft tissues surrounding the calvarial defect 6 weeks post-operation (Figure 7B). Histological observations at low magnification (40×) revealed that the implanted scaffolds were covered with abundant cells and tissue in both the uMSC-Exo and uMSC-Exo-miR-21+ groups, although a greater amount of callus tissue was observed on the scaffolds in the inner spaces of the uMSC-Exo-miR-21+ group. Moreover, the immunohistochemistry assay results showed that significantly more CD31-positive blood vessels formed in the uMSC-Exo-miR-21+ group. Compared with that in the control and uMSC-Exo groups, the expression of VEGFA in the new callus tissue was upregulated in the uMSC-Exo-miR-21+ group. Unsurprisingly, the expression of SPRY1 in the uMSC-Exo-miR-21+ group was decreased. These results were consistent with the results from our cell experiments, implying that exosomal miR-21 delivery stimulated greater vessel formation within callus regions and enhanced bone formation in the defect space.

Discussion

Our primary study confirmed that exosomes derived from uMSCs are beneficial to fracture healing in both a cell culture model and a well-established clinically relevant rat model of fracture. Interestingly, we found that in the process of promoting fracture healing, but not in regulating osteoblast proliferation, uMSC-Exos played a more important angiogenic role[13]. In the field of fracture healing, one of the most critical factors for union is sufficient blood supply at the fracture site[2]. Angiogenesis is observed before osteogenesis and continues throughout the entire healing process[2, 24]. Thus, promoting angiogenesis immediately after trauma is urgent and even critical. Therefore, in this paper, we provide the demonstration of the mechanism underlying the ability of uMSC-Exos to promote angiogenesis.

As intercellular communication is required for various physiological and pathological processes, exosomes can be readily isolated from MSCs of various origin, and these exosomes carry biologically active molecules (protein, microRNA, and DNA) that can be transferred to target cells to exert therapeutic effects[17]. Current research has indicated that the transfer of miRNAs delivered by exosomes to recipient cells is a novel mechanism[25]. Herein, we analysed the global expression of miRNAs in uMSC-Exos via high-throughput sequencing and miR-21 was found in greater abundance in both the uMSC-Exos and uMSCs groups than it was in the control group. Moreover, the expression of miR-21 in the HUVECs was significantly increased following treatment with uMSC-Exos. The immunofluorescence results indicated that exosomal miR-21 was indeed transferred to the HUVECs. As reported in the literature, miR-21 is frequently overexpressed in human cancers and acts as an oncogene, and it also plays a regulatory role in endothelial cell proliferation and migration and influences angiogenesis by interacting with hypoxia inducible factor 1 alpha (HIF-1α) or other factors[26–28]. Thus, in this study, we hypothesize that

exosomal miR-21, the most abundant miRNA in the uMSC-Exos, was the main transmitter of cellular information.

To confirm the role of exosomal miR-21 in this process, we transfected an inhibitor of miR-21 into uMSCs, extracted the exosomes, and determined the expression level of miR-21 in these exosomes. The expression decreased correspondingly, and subsequent tests showed a trend of proliferation and migration suppression when the HUVECs were co-cultivated with uMSC-Exo with a miR-21 inhibitor. Finally, the pro-angiogenesis function of HUVECs was also confirmed, and the results showed that exosomal miR-21 from uMSCs played a crucial angiogenic role in the HUVECs. However, details on the downstream pathway remain to be provided.

Bioinformatics analyses and luciferase assays were used to confirm that miR-21 binds directly to the 3'-UTR of the SPRY1 mRNA and inhibits the transcription of SPRY1. SPRY1 was previously described as a potent angiogenesis inhibitor in endothelial cells[29] and was found to inhibit the ERK/MAPK signalling induced by bFGF and VEGF[30–32]. Recent studies have shown that miR-21 contributes to the proliferation, migration, and apoptosis of cancer cells with the concomitant degradation of SPRY1[33, 34]. However, rarely is focused on the mechanism of miR-21 targeting of SPRY1 during angiogenesis or fracture healing. Our qRT-PCR and Western blot data showed that the mRNA level of SPRY1 increased dramatically when uMSC-Exos with miR-21 inhibitor were transfected into HUVECs. The mRNA expression of VEGFA and HIF-1α and the phosphorylation of AKT in the HUVECs were significantly decreased. It is reported that VEGF plays an important role in the endothelial cell mitosis and blood vessels fusion, thereby promoting neovascularization. HIF-1 exhibits enhanced stability under hypoxic conditions and regulates VEGF expression through transcriptional activation [29]. AKT is a well-characterized target of PI3K, and AKT phosphorylation is essential for the activation of the PI3K/AKT pathway[35, 36]. In the context of angiogenesis, accumulating evidence from a number of studies has shown that the PI3K/AKT signalling pathway plays a key role in ischaemic injury and the expression of multiple angiogenic molecules, such as VEGF and SDF-1, may be upregulated in this pathway[31, 37, 38]. To confirm that angiogenesis depends on SPRY1, we also used siRNA to inhibit the expression of SPRY1 in HUVECs. The qRT-PCR and Western blot analysis results showed that SPRY1 siRNA significantly inhibited the expression of HIF-1α and VEGF as well as PI3K/AKT pathway components. In addition, a series of results on cell function suggested that the angiogenic ability of HUVECs had been restricted. In accordance with these findings, the miR-21-dependent regulation of endothelial cell activity and angiogenesis were regulated by the activation of PI3K/AKT signalling upon downregulation of SPRY1.

The calvarial defect model is commonly used for studying bone formation[15]. To make our experimental results more convincing, we studied micro-vessels and bone formation in vivo. The role of exosomal miR-21 was evaluated by testing its ability in calvarial defect repair in a rat model. The restoration of blood flow is critical in bone formation not only for the transport of oxygen and nutrient but also for the initiation of ossification and recruitment of MSCs[2, 39]. Therefore, it was not surprising that the uMSC-Exo-induced formation of micro-vessel networks promoted bone healing in the calvarial defect, which has been observed in the previously studied femur fracture model[13]. In the current model, newly formed

vessels in the defect area were observed more clearly through three-dimensional images of the radiopaque contrast-filled vascular network. Moreover, the results from the in vivo study not only verified our hypothesis that a SPRY1-dependant mechanism involving exosomal-miR-21 induces angiogenesis but also indicated that the trends of significant in vivo microvascular remodelling and osseous regeneration lend substantial credibility to the utilization of uMSC-Exos and exosomal miR-21 in the development of future therapeutic tissue remodelling strategies.

In this research, we demonstrates a potential role for exosomal miR-21, additional studies are expected to determine the overall importance of exosomal miR-21 compared to the wider secretome and identify the deeper interactional mechanisms underlying exosome-related angiogenesis and osteogenesis.

Conclusions

Taken together, the findings from our current study indicate that the specific miR-21, which is shuttled directly from uMSCs to HUVECs via exosomes, regulates HUVEC proliferation, migration and tube formation through the activation of the PI3K/AKT pathway and induction of HIF-1α and VEGFA expression by suppressing the target gene SPRY1. Furthermore, a cranial defect model was utilized to verify this pro-angiogenic phenomenon and its impact on bone formation (Figure 8). Overall, the data presented herein provide the first evidence of a novel mechanism of exosomal miR-21 in inducing angiogenesis, which may provide a basis for prospective therapeutic approaches in the treatment of atrophic delayed or non-union fracture in the future.

Declarations

Ethical Approval and Consent to participate:

The feeding of allmice were performed at Shanghai Model Organisms (SCXK [Shanghai] 2017-0010 and SYXK [Shanghai] 2017-0012). The mice were kept in SPF facilities with no more than 5 in a cage with food and water available ad libitum. The protocols are in compliance with the regulations of the ethical committee of Shanghai Changhai Hospital.

Consent for publication:

Written informed consent for publication was obtained from all participants.

Availability of supporting data:

This study includes no data deposited in external repositories.

Competing interests:

The authors have declared that they have no competing interests.

Funding:

This study was supported by grants from the National Natural Science Foundation of China (Grant No. 81601890 and 81701923)

Author contributions:

YZ, XL, SF and SX designed this study and analysed the data. YZ and YX conducted the majority of the experiments and completed the manuscript. PW participated in the experimental design and the manuscript writing. YX, ZH and YX collected animal model samples. ZH and YX participated in editing the manuscript. All authors approved the final version of the manuscript.

Acknowledgements:

The authors thank Zhang Hao for assistance with Micro-CT assay.

Abbreviations:

Mesenchymal stem cells (MSC), umbilical cord mesenchymal stem cells (uMSC), human umbilical cord vein endothelial cells (HUVECs), exosomes (Exos),

References

1. Claes L, Recknagel S, Ignatius A. Fracture healing under healthy and inflammatory conditions. Nat Rev Rheumatol. 2012;8:133–43.
2. Einhorn TA, Gerstenfeld LC. Fracture healing: mechanisms and interventions. Nat Rev Rheumatol. 2015;11:45–54.
3. Gómez-Barrena E, Rosset P, Müller I, Giordano R, Bunu C, Layrolle P, Konttinen YT, Luyten FP. Bone regeneration: stem cell therapies and clinical studies in orthopaedics and traumatology. J Cell Mol Med. 2011;15:1266–86.
4. Antonova E, Le TK, Burge R, Mershon J. Tibia shaft fractures: costly burden of nonunions. BMC Musculoskelet Disord. 2013;14:42.
5. Hajnovic L, Sefranek V, Schütz L. Influence of blood supply on fracture healing of vertebral bodies. Eur J Orthop Surg Traumatol. 2018;28:373–80.
6. Rupp M, Biehl C, Budak M, Thormann U, Heiss C, Alt V. Diaphyseal long bone nonunions - types, aetiology, economics, and treatment recommendations. Int Orthop. 2018;42:247–58.

7. Infante A, Rodríguez CI. Osteogenesis and aging: lessons from mesenchymal stem cells. Stem Cell Res Ther. 2018;9:244.
8. Bartold M, Gronthos S, Haynes D, Ivanovski S. Mesenchymal stem cells and biologic factors leading to bone formation. J Clin Periodontol. 2019;46 Suppl 21:12–32.
9. Amariglio N, Hirshberg A, Scheithauer BW, Cohen Y, Loewenthal R, Trakhtenbrot L, Paz N, Koren-Michowitz M, Waldman D, Leider-Trejo L, Toren A, Constantini S, Rechavi G. Donor-derived brain tumor following neural stem cell transplantation in an ataxia telangiectasia patient. PLoS Med. 2009;6:e1000029.
10. Herberts CA, Kwa MS, Hermsen HP. Risk factors in the development of stem cell therapy. J Transl Med. 2011;9:29.
11. Li Y, Jin D, Xie W, Wen L, Chen W, Xu J, Ding J, Ren D, Xiao Z. Mesenchymal Stem Cells-Derived Exosomes: A Possible Therapeutic Strategy for Osteoporosis. Curr Stem Cell Res Ther. 2018;13:362–8.
12. Zhang W, Bai X, Zhao B, Li Y, Zhang Y, Li Z, Wang X, Luo L, Han F, Zhang J, Han S, Cai W, Su L, Tao K, Shi J, Hu D. Cell-free therapy based on adipose tissue stem cell-derived exosomes promotes wound healing via the PI3K/Akt signaling pathway. Exp Cell Res. 2018;370:333–42.
13. Zhang Y, Hao Z, Wang P, Xia Y, Wu J, Xia D, Fang S, Xu S. Exosomes from human umbilical cord mesenchymal stem cells enhance fracture healing through HIF-1α-mediated promotion of angiogenesis in a rat model of stabilized fracture. Cell Prolif. 2019;52:e12570.
14. Furuta T, Miyaki S, Ishitobi H, Ogura T, Kato Y, Kamei N, Miyado K, Higashi Y, Ochi M. Mesenchymal Stem Cell-Derived Exosomes Promote Fracture Healing in a Mouse Model. Stem Cells Transl Med. 2016;5:1620–30.
15. Qi X, Zhang J, Yuan H, Xu Z, Li Q, Niu X, Hu B, Wang Y, Li X. Exosomes Secreted by Human-Induced Pluripotent Stem Cell-Derived Mesenchymal Stem Cells Repair Critical-Sized Bone Defects through Enhanced Angiogenesis and Osteogenesis in Osteoporotic Rats. Int J Biol Sci. 2016;12:836–49.
16. Carmeliet P, Jain RK. Molecular mechanisms and clinical applications of angiogenesis. Nature. 2011;473:298–307.
17. Couzin J. Cell biology: The ins and outs of exosomes. Science. 2005;308:1862–3.
18. Fang S, Xu C, Zhang Y, Xue C, Yang C, Bi H, Qian X, Wu M, Ji K, Zhao Y, Wang Y, Liu H, Xing X. Umbilical Cord-Derived Mesenchymal Stem Cell-Derived Exosomal MicroRNAs Suppress Myofibroblast Differentiation by Inhibiting the Transforming Growth Factor-β/SMAD2 Pathway During Wound Healing. Stem Cells Transl Med. 2016;5:1425–39.
19. Zhang J, Li S, Li L, Li M, Guo C, Yao J, Mi S. Exosome and exosomal microRNA: trafficking, sorting, and function. Genomics Proteomics Bioinformatics. 2015;13:17–24.
20. Sun Z, Shi K, Yang S, Liu J, Zhou Q, Wang G, Song J, Li Z, Zhang Z, Yuan W. Effect of exosomal miRNA on cancer biology and clinical applications. Mol Cancer. 2018;17:147.
21. Trajkovic K, Hsu C, Chiantia S, Rajendran L, Wenzel D, Wieland F, Schwille P, Brügger B, Simons M. Ceramide triggers budding of exosome vesicles into multivesicular endosomes. Science.

2008;319:1244–7.

22. Catalano M, O'Driscoll L. Inhibiting extracellular vesicles formation and release: a review of EV inhibitors. J Extracell Vesicles. 2020;9:1703244.
23. Calvisi DF, Ladu S, Gorden A, Farina M, Lee JS, Conner EA, Schroeder I, Factor VM, Thorgeirsson SS. Mechanistic and prognostic significance of aberrant methylation in the molecular pathogenesis of human hepatocellular carcinoma. J Clin Invest. 2007;117:2713–22.
24. Brownlow HC, Reed A, Simpson AH. The vascularity of atrophic non-unions. Injury. 2002;33:145–50.
25. Raposo G, Stoorvogel W. Extracellular vesicles: exosomes, microvesicles, and friends. J Cell Biol. 2013;200:373–83.
26. An Y, Zhao J, Nie F, Qin Z, Xue H, Wang G, Li D. Exosomes from Adipose-Derived Stem Cells (ADSCs) Overexpressing miR-21 Promote Vascularization of Endothelial Cells. Sci Rep. 2019;9:12861.
27. Du X, Hong L, Sun L, Sang H, Qian A, Li W, Zhuang H, Liang H, Song D, Li C, Wang W, Li X. miR-21 induces endothelial progenitor cells proliferation and angiogenesis via targeting FASLG and is a potential prognostic marker in deep venous thrombosis. J Transl Med. 2019;17:270.
28. Zhang Y, Yuan F, Liu L, Chen Z, Ma X, Lin Z, Zou J. The Role of the miR-21/SPRY2 Axis in Modulating Proangiogenic Factors, Epithelial Phenotypes, and Wound Healing in Corneal Epithelial Cells. Invest Ophthalmol Vis Sci. 2019;60:3854–62.
29. Tabruyn SP, Sabatel C, Nguyen NQ, Verhaeghe C, Castermans K, Malvaux L, Griffioen AW, Martial JA, Struman I. The angiostatic 16K human prolactin overcomes endothelial cell anergy and promotes leukocyte infiltration via nuclear factor-kappaB activation. Mol Endocrinol. 2007;21:1422–9.
30. Impagnatiello MA, Weitzer S, Gannon G, Compagni A, Cotten M, Christofori G. Mammalian sprouty-1 and – 2 are membrane-anchored phosphoprotein inhibitors of growth factor signaling in endothelial cells. J Cell Biol. 2001;152:1087–98.
31. Zhang Z, Yao L, Yang J, Wang Z, Du G. PI3K/Akt and HIF–1 signaling pathway in hypoxia–ischemia (Review). Mol Med Rep. 2018;18:3547–54.
32. Gross I, Bassit B, Benezra M, Licht JD. Mammalian sprouty proteins inhibit cell growth and differentiation by preventing ras activation. J Biol Chem. 2001;276:46460–8.
33. Ning ZW, Luo XY, Wang GZ, Li Y, Pan MX, Yang RQ, Ling XG, Huang S, Ma XX, Jin SY, Wang D, Li X. MicroRNA-21 Mediates Angiotensin II-Induced Liver Fibrosis by Activating NLRP3 Inflammasome/IL-1β Axis via Targeting Smad7 and Spry1. Antioxid Redox Signal. 2017;27:1–20.
34. Mao XH, Chen M, Wang Y, Cui PG, Liu SB, Xu ZY. MicroRNA-21 regulates the ERK/NF-κB signaling pathway to affect the proliferation, migration, and apoptosis of human melanoma A375 cells by targeting SPRY1, PDCD4, and PTEN. Mol Carcinog. 2017;56:886–94.
35. Janku F, Yap TA, Meric-Bernstam F. Targeting the PI3K pathway in cancer: are we making headway. Nat Rev Clin Oncol. 2018;15:273–91.
36. Rahmani F, Ferns GA, Talebian S, Nourbakhsh M, Avan A, Shahidsales S. Role of regulatory miRNAs of the PI3K/AKT signaling pathway in the pathogenesis of breast cancer. Gene. 2020;737:144459.

37. Quan XJ, Liang CL, Sun MZ, Zhang L, Li XL. Overexpression of steroid receptor coactivators alleviates hyperglycemia-induced endothelial cell injury in rats through activating the PI3K/Akt pathway. Acta Pharmacol Sin. 2019;40:648–57.
38. Kar S, Samii A, Bertalanffy H. PTEN/PI3K/Akt/VEGF signaling and the cross talk to KRIT1, CCM2, and PDCD10 proteins in cerebral cavernous malformations. Neurosurg Rev. 2015;38:229–36. discussion 236–237.
39. Song D, He G, Song F, Wang Z, Liu X, Liao L, Ni J, Silva MJ, Long F. Inducible expression of Wnt7b promotes bone formation in aged mice and enhances fracture healing. Bone Res. 2020;8:4.

Figures

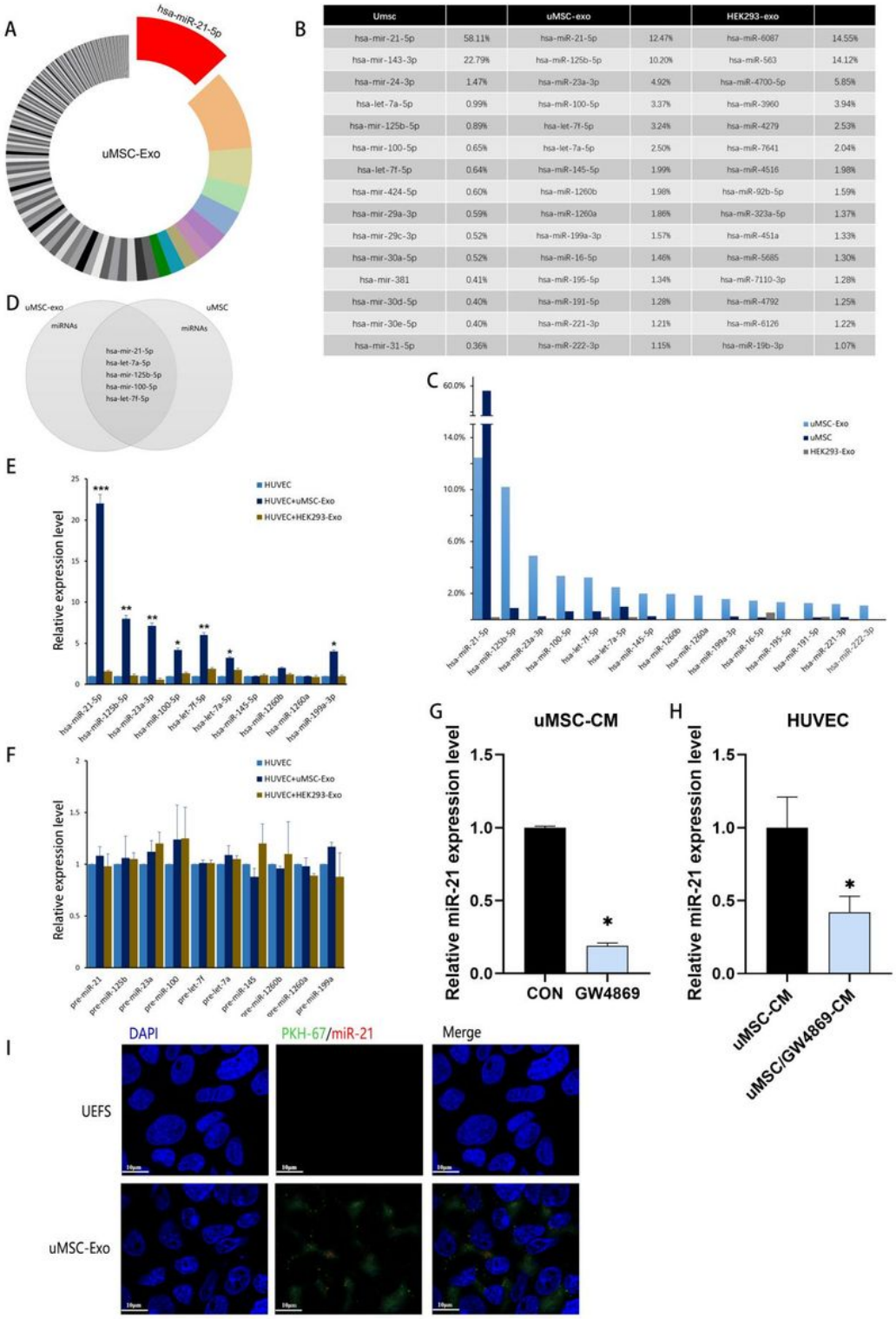

Umsc		uMSC-exo		HEK293-exo	
hsa-mir-21-5p	58.11%	hsa-miR-21-5p	12.47%	hsa-miR-6087	14.55%
hsa-mir-143-3p	22.79%	hsa-miR-125b-5p	10.20%	hsa-miR-563	14.12%
hsa-mir-24-3p	1.47%	hsa-miR-23a-3p	4.92%	hsa-miR-4700-5p	5.85%
hsa-let-7a-5p	0.99%	hsa-miR-100-5p	3.37%	hsa-miR-3960	3.94%
hsa-mir-125b-5p	0.89%	hsa-let-7f-5p	3.24%	hsa-miR-4279	2.53%
hsa-mir-100-5p	0.65%	hsa-let-7a-5p	2.50%	hsa-miR-7641	2.04%
hsa-let-7f-5p	0.64%	hsa-miR-145-5p	1.99%	hsa-miR-4516	1.98%
hsa-mir-424-5p	0.60%	hsa-miR-1260b	1.98%	hsa-miR-92b-5p	1.59%
hsa-mir-29a-3p	0.59%	hsa-miR-1260a	1.86%	hsa-miR-323a-5p	1.37%
hsa-mir-29c-3p	0.52%	hsa-miR-199a-3p	1.57%	hsa-miR-451a	1.33%
hsa-mir-30a-5p	0.52%	hsa-miR-16-5p	1.46%	hsa-miR-5685	1.30%
hsa-mir-381	0.41%	hsa-miR-195-5p	1.34%	hsa-miR-7110-3p	1.28%
hsa-mir-30d-5p	0.40%	hsa-miR-191-5p	1.28%	hsa-miR-4792	1.25%
hsa-mir-30e-5p	0.40%	hsa-miR-221-3p	1.21%	hsa-miR-6126	1.22%
hsa-mir-31-5p	0.36%	hsa-miR-222-3p	1.15%	hsa-miR-19b-3p	1.07%

Figure 1

Specific miRNA abundance signatures in exosomes derived from the uMSCs (A) Pie chart of the exosomal miRNA abundance analysis by high-throughput small RNA sequencing. The top 10 most abundant miRNAs in uMSC-derived exosomes are colour labelled. The miR-21 constituted the largest proportion. (B, C) Top 10 most abundant miRNA in the uMSCs, uMSC-Exos and HEK293-Exos. (D) Intersection diagram showing miR-21-5p, miR-100-5p, miR-125b-5p, and let-7f-5p, which are among the

top 10 most abundant miRNAs in both the uMSCs and uMSC-Exos. (E) qRT-PCR results show the 10 most abundant miRNAs in uMSC-Exos and their pre-miRNA expression levels in the HUVECs subjected to interference for 48 h. (F) Results show that the expression of miR-21-5p in the uMSC-Exo group was significantly increased compared with that in the HEK293-Exos group, while the pre-miRNAs were not affected. (G) Exosome inhibitor (GW4869) was used to test whether miR-21 was transferred to the target cells by exosomes. The expression of miR-21 in the uMSCs in CM treated with GW4869 was significantly decreased compared with that in the uMSCs in CM obtained from the control uMSCs. (H) Expression of miR-21 in the HUVECs treated with GW4869-CM for 48 h was also significantly decreased compared to that in the HUVECs treated with uMSC-CM. (I) Immunofluorescence shows that the green exosomes (stained with PKH67 fluorescent dye) are mainly concentrated near the nucleus (DAPI). The merged image shows that the location of the miR-21 (red spots) is consistent with that of the exosomes. However, neither exosomes nor miRNA components were detected in the uMSC-Exo-free supernatant (UEFS). Data are presented as the means±SD; *$p<0.05$; **$p<0.01$; ***$p<0.001$

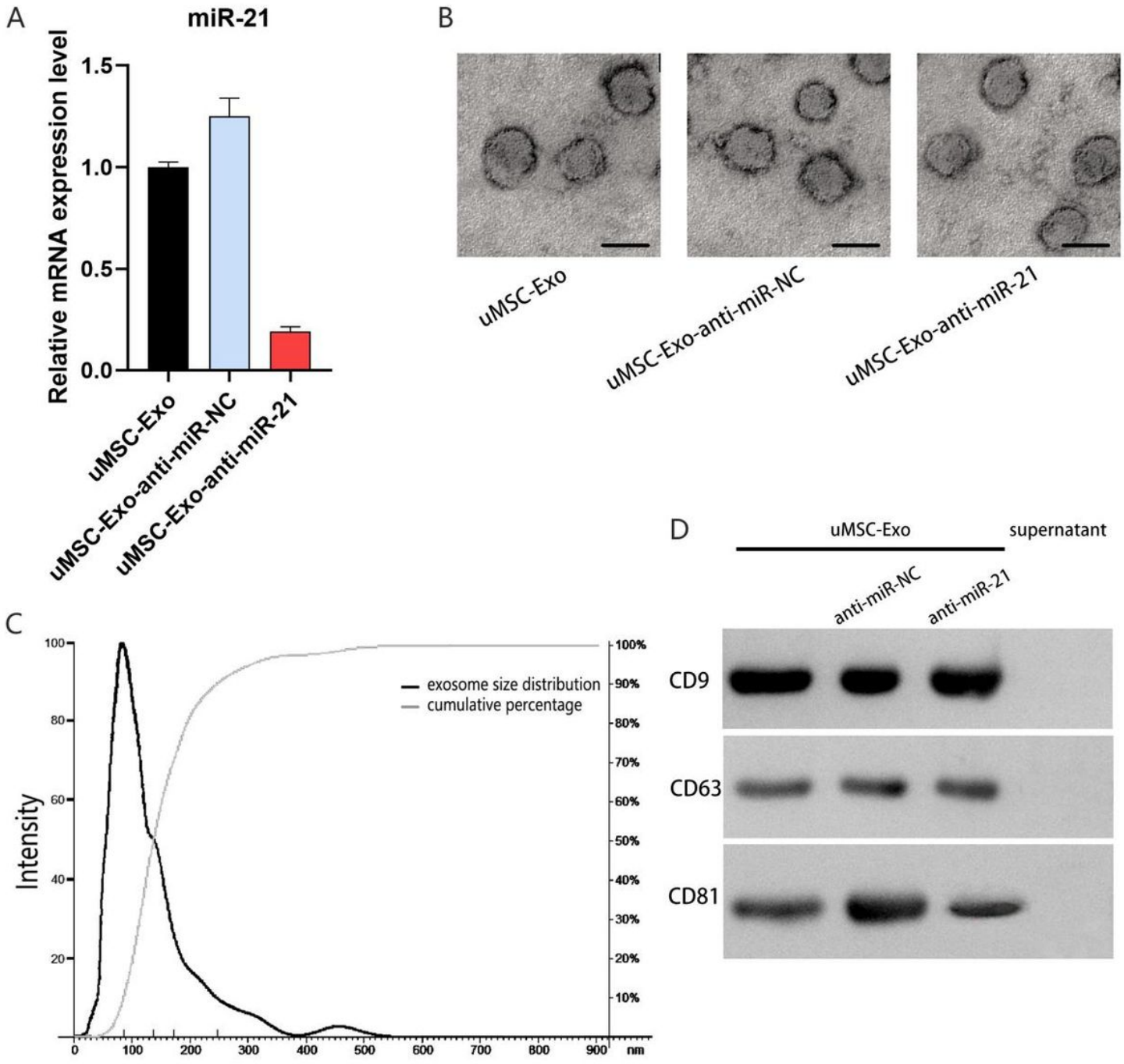

Figure 2

Extraction and identification of the exosomes (A) qRT-PCR was performed to analyse the relative miR-21 levels in HUVECs after the miR-21 inhibitor was transfected into uMSC-Exos. (B) Morphology of each group of exosomes photographed via TEM. Scale bar: 100 nm. (C) Size distribution of the exosomes was determined with a NanoSight LM10 instrument. (D) Western blot analysis of CD9, CD63 and CD81 in the exosomes.

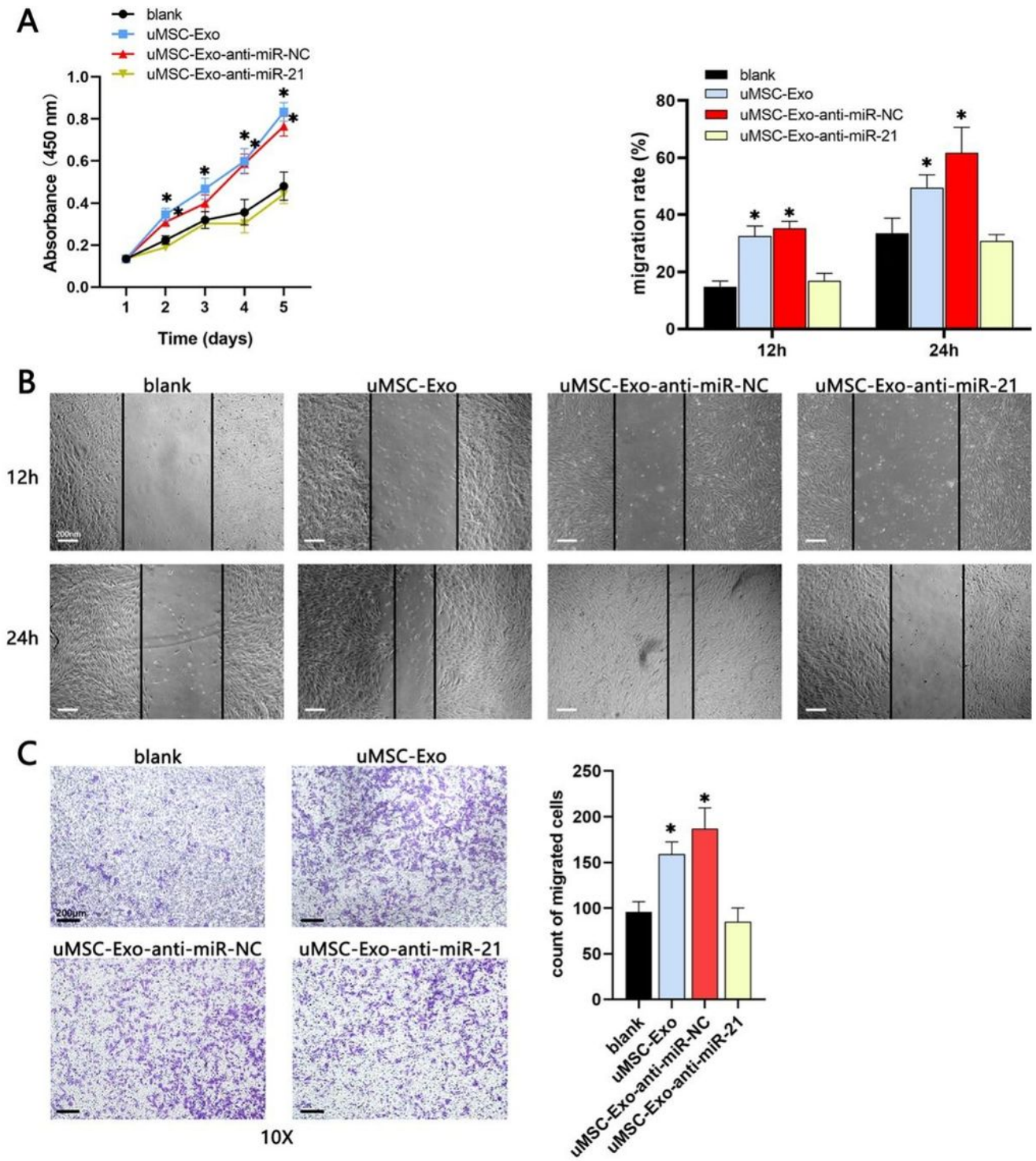

Figure 3

Effects of uMSC-Exo-anti-miR-21 on the proliferation and migration of the HUVECs (A) CCK8 assay was used to evaluate the HUVEC proliferation rate after uMSC-Exo-anti-miR-NC, uMSC-Exo-anti-miR-21 or uMSC-Exos treatment. A group of HUVECs with PBS treatment served as the blank. uMSC-Exos promoted HUVEC proliferation, and this effect was attenuated by miR-21 inhibition. (n=3 per group). (B) Extracted exosomes promoted cell migration as determined by a scratch test at 0 h, 12 h and 24 h after treatment.

At the same time point (12 h or 24 h), although the number of migrating cells in the uMSC-Exo-anti-miR-21 group was increased, the rate was significantly slower than that of the other two groups (uMSc-Exo and uMEC-Exo-anti-miR-NC groups). (C) Transwell experiments showed that the number of migrating HUVECs was reduced by approximately one-half after exposure to exosome inhibitors. Data are presented as the means±SD; *p<0.05.

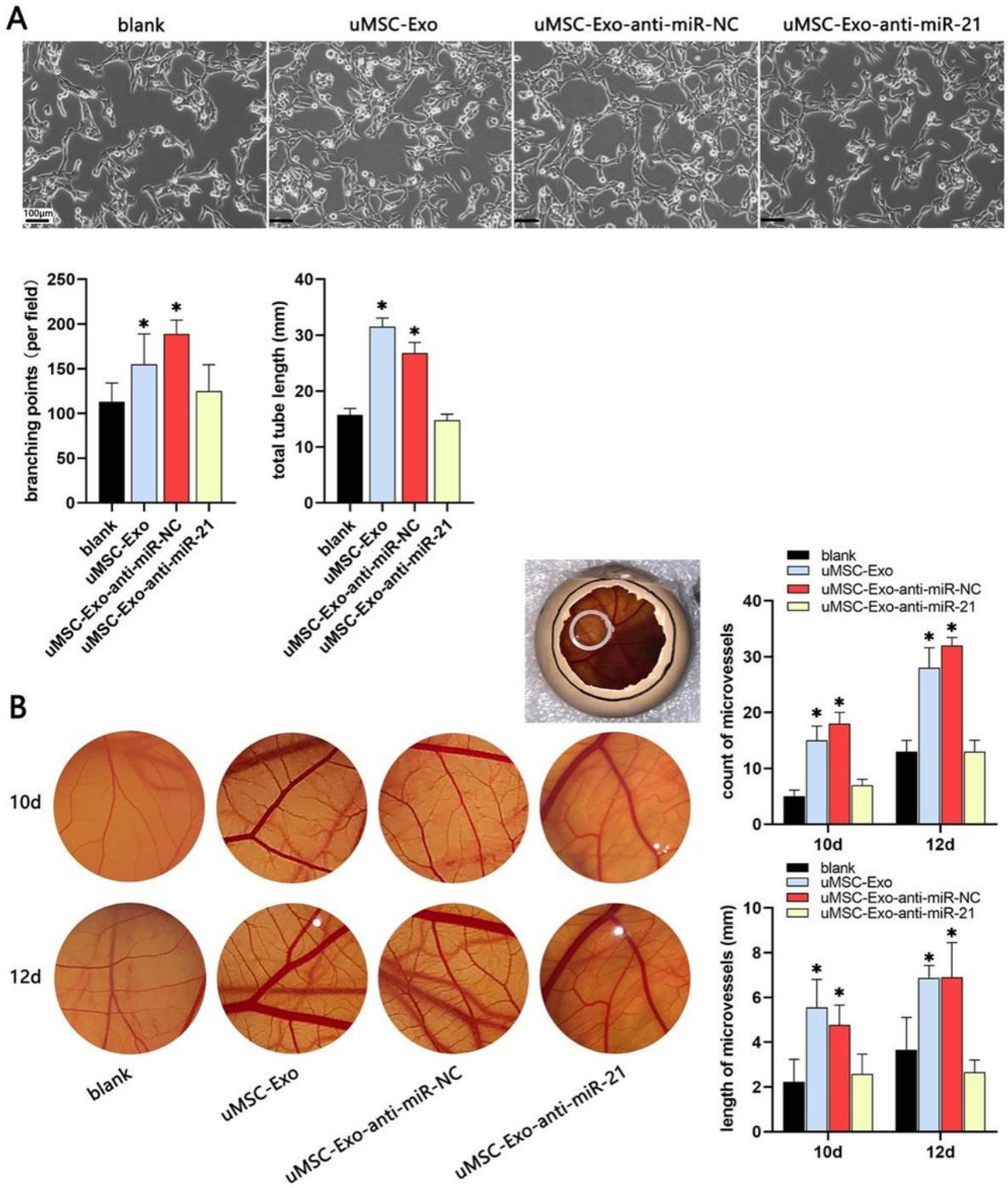

Figure 4

Effects of uMSC-Exo-anti-miR-21 on the pro-angiogenesis of the HUVECs (A) Tube formation assay performed to determine the extent of in vitro angiogenesis, and the results showed growing branch points and tube elongation in the uMSC-Exo group and uMSC-Exo-anti-miR-NC group as well as in the uMSC-Exo-anti-miR-21 group and blank group in a time-dependent manner. Compared with that of the other two groups, the uMSC-Exo group treated with inhibitors of miR-21 and the blank group had the lowest growth rates. (B) Chicken chorioallantoic membrane (CAM) assay results showed that uMSC-Exo-anti-miR-21 was able to impair in ovo neovascularization, which was decreased two-fold compared to that of the other two groups on the tenth day. In addition, at the following time points, it continued to increase at a lower rate than the two control groups. Data are presented as the means±SD; *$p<0.05$.

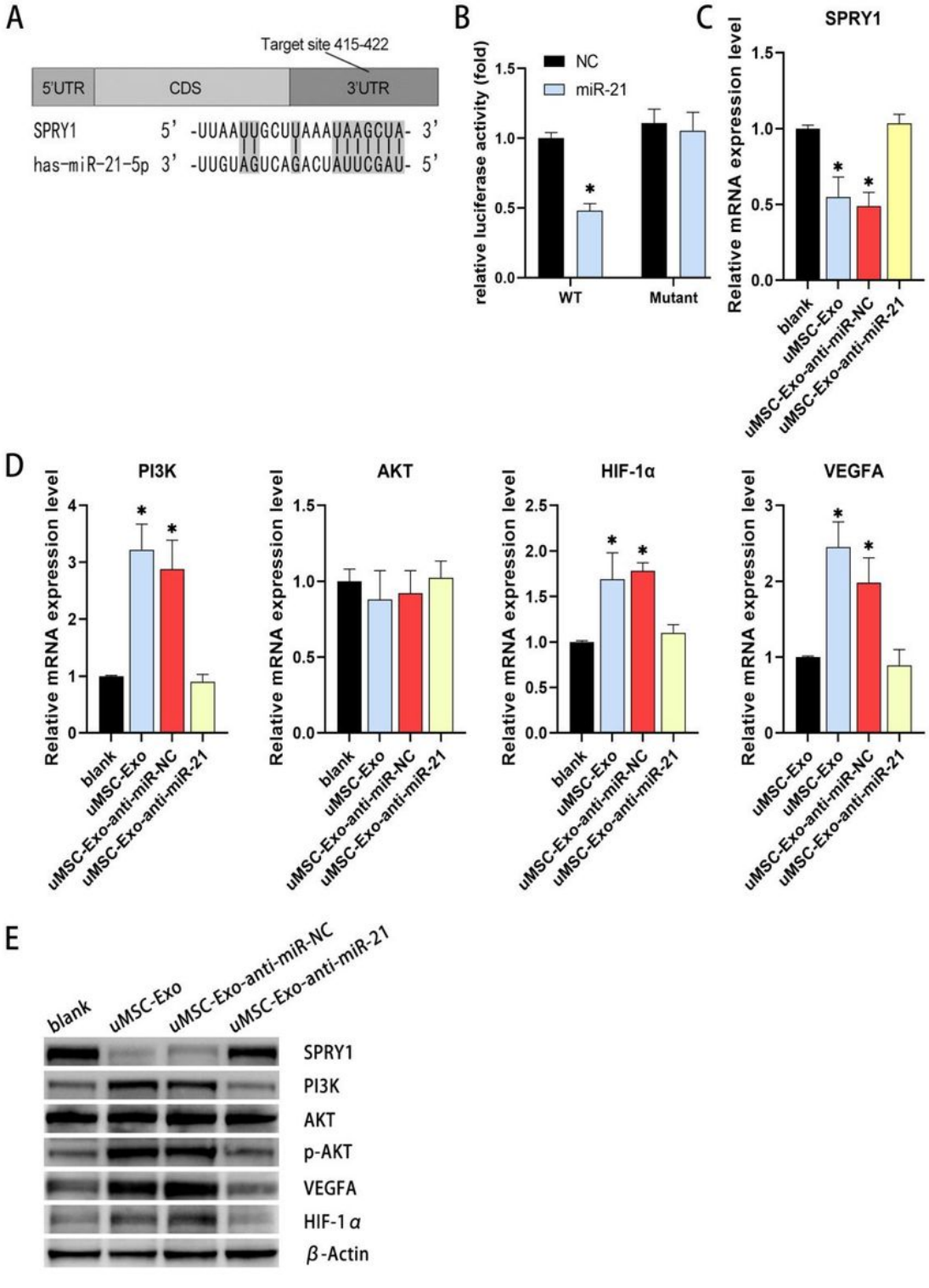

Figure 5

Exosomal miR-21 derived from uMSCs activates PI3K/AKT signalling by targeting SPRY1 in the HUVECs (A) Schematic representation of the putative binding sites for miR-21-5p in the SPRY1 3'-UTR. Predicted consequential pairings of the target regions and miR-21 (underlined) were based on data from TargetScan (www.targetscan.org). (B) Luciferase reporters containing wild-type or mutant 3'-UTR of SPRY1 genes were co-transfected with miR-21-NC or miR-21 mimics into HEK293 cells. Two days after

transfection, the dual luciferase activity was measured. (C) qRT-PCR was performed to measure the mRNA level of SPRY1, and the results showed that the highest expression level was in the uMSC-Exo-anti-miR-21 group. (D) Downstream genes were shown to be PI3K, AKT VEGFA and HIF-1α in the HUVECs transfected with uMSC-Exo-anti-miR-NC, uMSC-Exo-anti-miR-21 or uMSC-Exos (negative control). Except for AKT, which did not change, the expression of these mRNAs was decreased by approximately two-fold in the uMSC-Exo-anti-miR-21 group. (E) Western blotting analysis results of PI3K, SPRY1, VEGFA, HIF-1α, p-AKT, and AKT show that the uMSC-Exos and uMSC-Exo-anti-miR-NC treatments enhanced the protein levels of VEGFA, p-AKT, and HIF-1α and reduced the protein levels of SPRY1, while the opposite results were found for the uMSC-Exo-anti-miR-21 group. However, the total AKT remained unchanged. The results were the same as those obtained by qRT-PCR. Data are presented as the means±SD; *$p<0.05$.

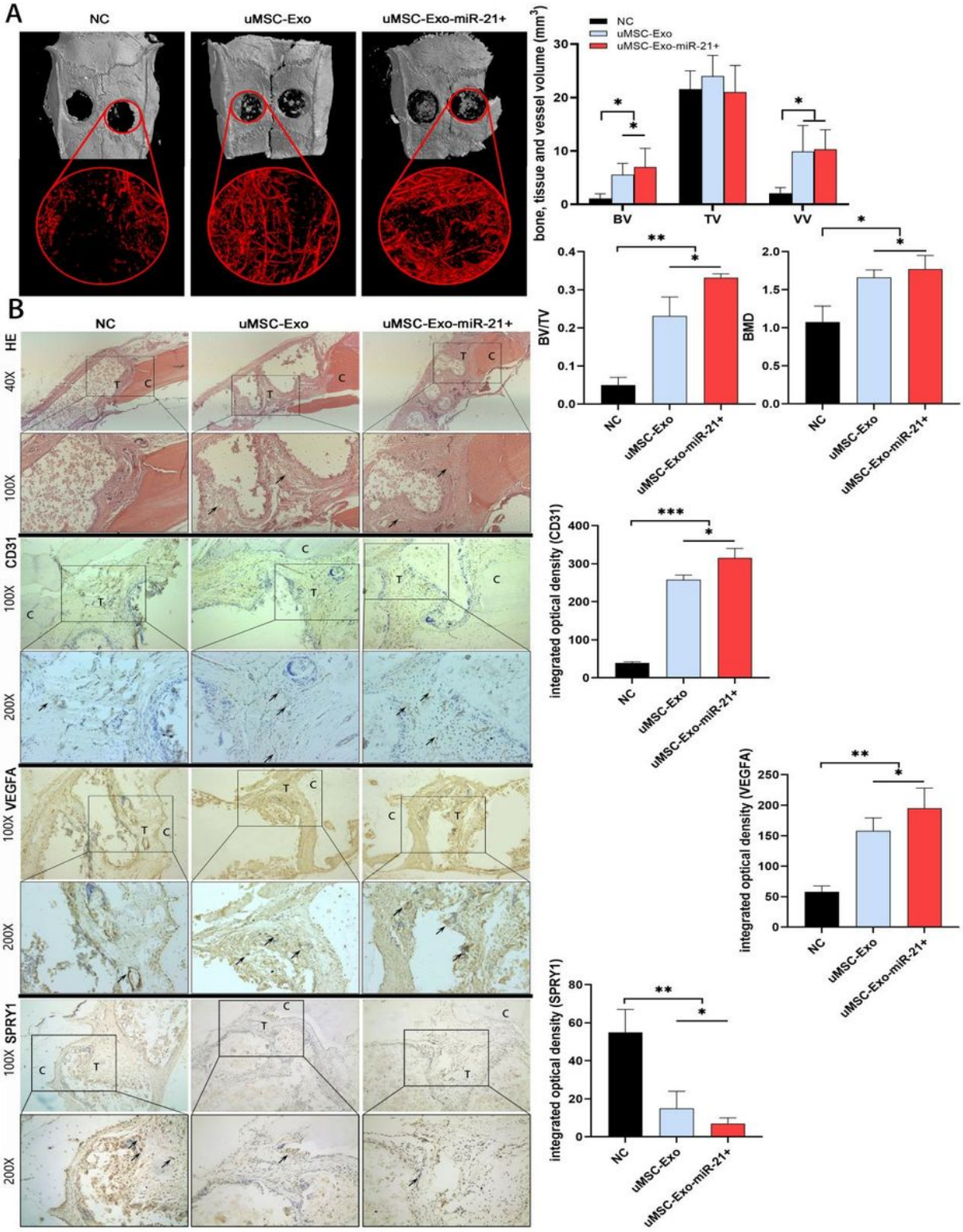

Figure 6

SPRY1 knockdown increases PI3K/AKT activation and HUVEC proliferation by adapting uMSC-Exos The inhibitory efficiency of siRNAs was tested by qRT-PCR (A) and Western blot (B). The decrease in SPRY1#1 was more apparent; therefore, SPRY1#1 was used for the downstream functional experiments. (C) After HUVECs were transfected with SPRY1, siRNA #1 was stimulated with uMSC-Exos for 24 h and the PI3K/AKT activation levels were determined by qRT-PCR. We observed a decrease in the level of PI3k,

VEGFA and HIF-1α in the uMSC-Exo+siRNA-SPRY1#1 group. However, the total AKT showed no change trend. (D) Western blot results suggested that the level of phosphorylated AKT in siRNA-SPRY1#1 was active. (E) Scratch experiment results showed that at the same time points (12 h and 24 h), the number of migrating cells in the two groups increased while those in the uMSC-Exo+siRNA-SPRY1#1 group migrated at a slower rate. (F) Tube formation data at the same time points showed the number of branches and blood vessels. The bar chart below shows that in the uMSC-Exo-siRNA-SPRY1#1 group, the branches and vessels were decreased more than two-fold. Data are presented as the means±SD; *p<0.05.

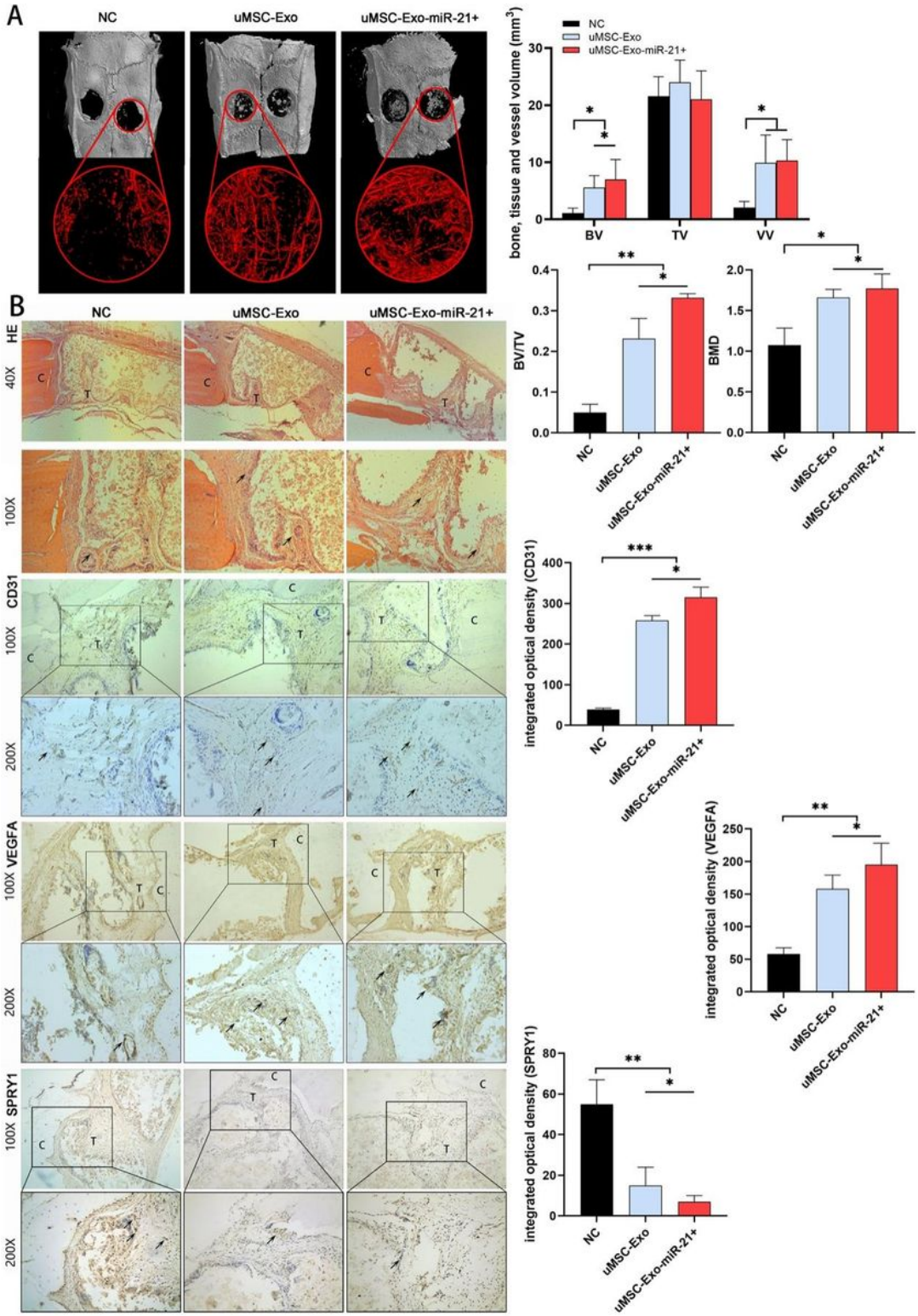

Figure 7

Exosomal miR-21 derived from uMSCs enhanced local microvascular network formation and bone regeneration in vivo. (A) Representative 3D reconstruction of images of calvarial bone defects taken 6 weeks after uMSC-Exo implantation (left) and morphometric analysis of the new bone volume (BV), tissue volume (TV), BV/TV, vessel volume (VV) and bone mineral density (BMD) as ascertained by micro-CT for each group 6 weeks post-operation (right). (B) Histological analysis results showed bone regeneration and angiogenesis as determined by haematoxylin and eosin (H&E) staining. H&E staining (40× and 100×) revealed that overexpressed exosomal miR-21 led to newly formed bone trabecula. Immunohistochemistry (100× and 200×) of the callus tissue showed that the positive expression of CD31 and VEGFA was increased while the expression of SPRY1 was decreased in the uMSC-Exo-miR-21+ group. C: calvarial bone; M: materials; T: tissues; arrow: positive immunostaining; and NC, negative control. Data are presented as the means±SD; *p<0.05.

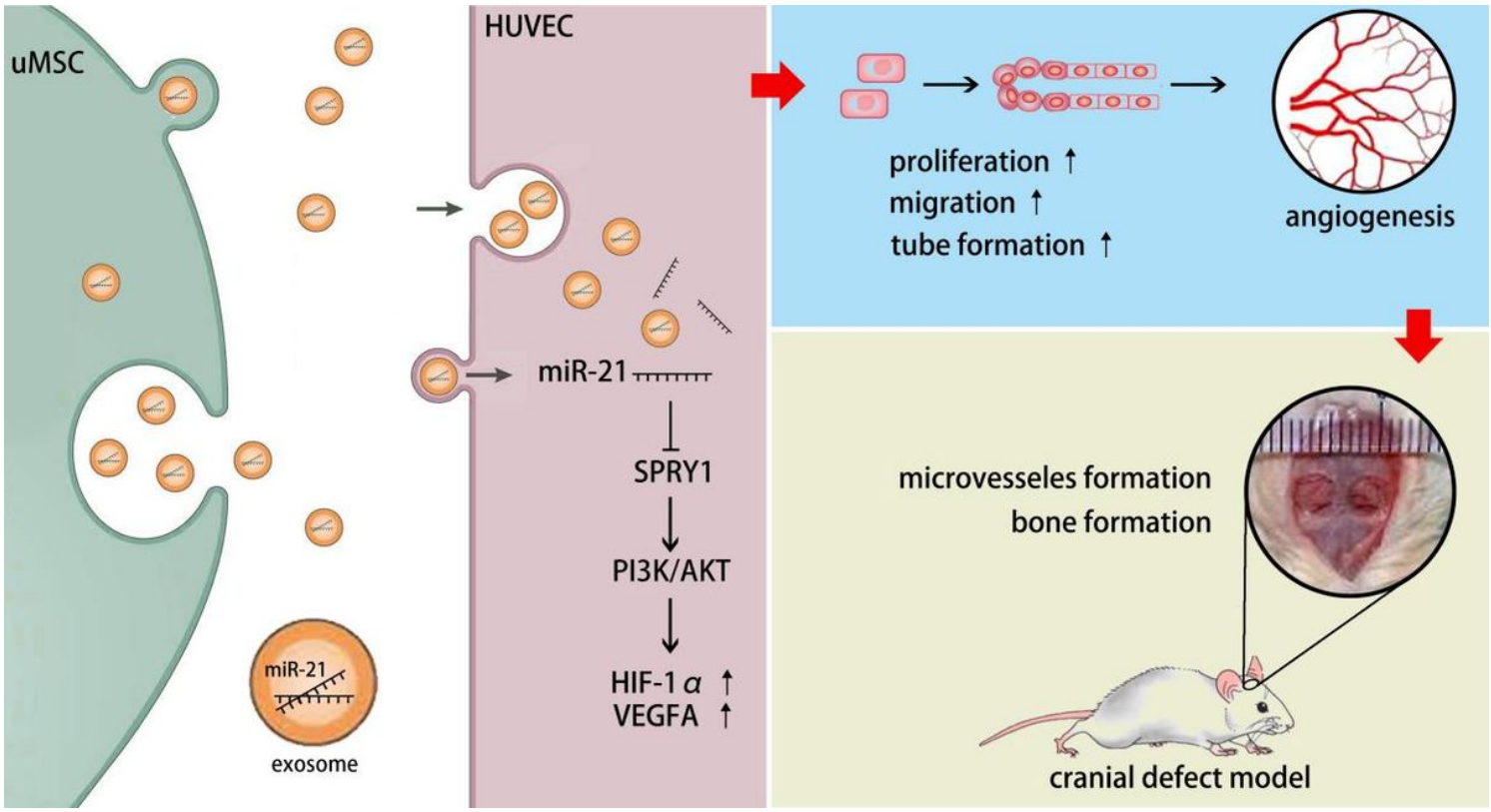

Figure 8

Schematic representation of proposed uMSC-Exo mechanism of action in bone repair and regeneration. The exosomal miR-21-mediated pro-angiogenesis roles in HUVECs and promoted blood vessels and bone formation in a cranial defect model.